TEOS Silane Film Modified with SBA-15 Loaded with Cocoa Husk Extract as Pretreatment of ASTM 1008 Steel

Iago M. F. C. R. e Silva[a], Gabriel A. Carrijo-Gonçalves[b], Lhaira S. Barreto[c], Luiz Carlos Salay[d],

Glória M. Vinhas[c], Idalina V. Aoki[b] ⓘD, Miriam S. Tokumoto[d], Vera R. Capelossi[a] ⓘD*

[a]Universidade Estadual de Santa Cruz, Departamento de Engenharia e Computação, Ilhéus, BA, Brasil.
[b]Universidade de São Paulo, Escola Politécnica, Departamento de Engenharia Química, São Paulo, SP, Brasil.
[c]Universidade Federal de Pernambuco, Departamento de Engenharia Química, Recife, PE, Brasil.
[d]Universidade Estadual de Santa Cruz, Departamento de Ciências Exatas, Ilhéus, BA, Brasil.

Research on eco-friendly methods led to the investigation of natural inhibitors and silane films modified with nanostructured mesoporous silica (SBA-15), a molecular sieve that can carry molecules with inhibitory properties. Combining natural extracts such as cocoa husk with SBA-15 aims to develop an enhanced silane-based pretreatment. This involves obtaining an alcoholic extract, and then mixing it with SBA-15 to modify the silane film. Different concentrations (1%, 2%, and 3%) of SBA-15 loaded with extract were prepared. Electrochemical tests, especially electrochemical impedance spectroscopy (EIS), in a 0.1 mol/L NaCl solution, revealed improved corrosion resistance with the tetraethylorthosilane (TEOS) film modified using 3% SBA-15 loaded with extract. Scanning electron microscopy showed the film and SBA-15 on the steel surface, while Fourier transform infrared spectroscopy identified functional groups characteristic of SBA-15, pure or loaded, and silane film. Therefore, it was possible to enhance the TEOS silane film by adding SBA-15 loaded with plant residue extract.

Keywords: *Pretreatment, Silane, Green inhibitor, SBA-15, Corrosion.*

1. Introduction

Carbon steel is widely used in industries such as oil and gas, petrochemical, nuclear, cellulose, and civil construction, for application in pipes, reactors, storage tanks, and concrete reinforcement, due to its properties such as low hardenability, excellent forgeability and weldability, in addition to its low cost[1,2]. However, this steel has low corrosion resistance when exposed to corrosive environments, especially in the presence of chlorides[1,3]. Thus, methods such as pretreatments and corrosion inhibitors are needed to provide greater resistance against corrosion, anchoring of future coatings, and active protection in aggressive media[4,5].

Pretreatments are processes that increase the service life of metallic material and improve the coupling of coatings such as paints[6]. Chromatization and phosphating are widely used commercial pretreatments, but they are harmful to the environment and human health[7]. Silanes are organofunctional molecules with organic and inorganic properties, such as TEOS (tetraethylorthosilane), acting as a coupling agent on the inorganic surface of the metal and organic surfaces of future coatings, being a potential sustainable substitute for commercial pretreatments[8].

Corrosion inhibitors must have antioxidant properties due to the presence of heteroatoms with unpaired electrons, such as S, O, N, or electron-donating π bonds that can interact with the free "d" orbitals of iron[9]. Agricultural residues including cocoa husk have attracted interest as natural corrosion inhibitors due to the presence of antioxidant molecules such as theobromine. This discovery presents a promising alternative to costly and potentially toxic commercial inhibitors[10,11].

The application of inhibitors in silane films can improve the barrier effect, in addition to promoting active protection by adsorption on the metallic surface, as already studied for natural sources such as mint leaf and caffeine[12,13]. The addition of other modifiers to silane films, such as rare earth salts, appears as an alternative to improve anticorrosive performance, coating anchoring and self-healing effect[14-16].

Nanotechnology is currently highlighted in the field of corrosion, for example, using catalyst supports or adsorbents[17-21] such as nanocontainers[22-25], carrying corrosion inhibitors or paint components to promote smart inhibitor adsorption or self-healing. The SBA-15 (Santa Bárbara Amorphous) is a mesoporous silica with a 2D hexagonal structure, it has excellent thermal stability, large pore volume, and surface area, in addition to having a low cost silicon source as a precursor, tetraethylorthosilane (TEOS), and a fast synthesis procedure when compared with other mesoporous materials[26-28]. The literature reports the loading of these mesoporous materials with compounds that have inhibitory properties[28,29]. Therefore, this study seeks to evaluate the TEOS silane film modified with SBA-15 loaded with cocoa husk alcoholic extract for carbon steel corrosion protection in 0.1 mol/L NaCl solution.

*e-mail: vera.rosa@gmail.com

2. Methodology

2.1. Inhibitor preparation

The preparation of the inhibitor followed the methodology proposed by Barreto et al.[11,30] e Carvalho et al.[31]. The cocoa husk, donated by Fazenda Bahia (Jitaúna-BA), was washed and dried at 60 °C until to a constant mass. Soon after the husk was ground in a knife mill (SPLABOR) and immersed in pure ethanol in a 1:2 ratio (%w) for 48 h, followed by vacuum filtration and extract formation using a rotary evaporator system (Fisatom 801) at 60 ºC.

2.2. Surface preparation

The ASTM 1008 steel sheets, donated by USIMINAS-MG, were cut with a guillotine to dimensions of 3 cm x 2 cm x 1 mm, after cleaning with cotton soaked in ethanol, followed by an ultrasonic bath with acetone for 10 min. Finally, they were cleaned with Saloclean 680RM alkaline degreaser (donated by Klintex Insumos Industriais) for 10 min at (60 ± 5) °C, washed with distilled water, and dried with a cold air jet.

2.3 SBA-15 synthesis.

The methodology for the synthesis of SBA-15 followed the sol-gel verified synthesis method by Meynen et al.[26], starting from the molar ratio 1 TEOS : 5.87 HCl : 194 H_2O : 0.017 P123 (pluronic). Initially, distilled water (H_2O), pluronic (P123), and hydrochloric acid (HCl) were mixed at 45 ºC and stirred until P123 was completely dissolved, then TEOS silane was added drop by drop. After 7.5 h of reaction, stirring was stopped, the temperature was raised to 80 °C, and the mixture was aged for 15.5 h. This mixture was vacuum filtered and successively washed with distilled water and ethanol. The retained material was dried at 100 °C for 2 h. Another washing step was carried out in the Soxhlet extractor for 24 h with ethanol followed by drying at 100 ºC for 2 h. Finally, the SBA-15 was obtained after calcining this material in a muffle furnace at 550 ºC with a heating rate of 1 ºC/min in the ambient atmosphere for 6 h and removed after natural cooling, as shown in Figure 1.

The loading of SBA-15 with the alcoholic extract of the cocoa husk was carried out by mixing 1% (%w) of SBA-15 in the extract under agitation for 24 h, immediately after vacuum filtration, washing with ethanol and drying at 60 °C for 1 h, obtaining the loaded SBA-15 (EXSBA).

2.4. Pretreatment with TEOS silane film

A solvent solution of water and ethanol 1:1 (%w) was prepared, acidified with glacial acetic acid until pH 4, added 1% (%w) of SBA-15 to evaluate pure silica or added 1%, 2%, or 3% (%w) of loaded SBA-15 and sent for an ultrasound for 10 min. After that, 4% (%v) of TEOS silane was added under stirring for hydrolysis for 75 min. The carbon steel was pretreated in a dip-coating process for 2 min of immersion and cured in an oven at 150 °C for 60 min.

2.5. X-ray diffraction analysis (XRD)

Pure SBA-15 (SBA) and SBA-15 loaded with natural inhibitor (EXSBA) were characterized by X-ray diffraction (XRD) using a Rigaku SmartLab instrument. Measurements were performed in the 2θ range from 0.5° to 80° for low-angle and high-angle measurements, with Cu Kα radiation and a step size of 0.02°, using an accelerating voltage of 40 kV and a current of 40 mA.

2.6. Thermogravimetric analysis (TGA)

The TGA measurements were performed on a METTLER TOLEDO TGA 2 Star System instrument at the Petrochemical Laboratory (LPQ) of the Federal University of Pernambuco (UFPE). The analyses used approximately 4 mg of the material in a 40 μL alumina crucible, and were subjected to heating in the temperature range of 35 °C to 800 °C which was heated in the temperature range of 10 °C/min. The atmosphere used was nitrogen (N_2), controlled with a flow of 50 mL/min.

2.7. Electrochemical tests

The electrochemical tests of films in the absence or modified with SBA or EXSBA in different concentrations, as well of bare steel (ASTM 1008), were obtained in a three-electrode electrochemical cell, being the working electrode the sample, with an exposed area of 1 cm^2, the reference electrode Ag/AgCl/KCl$_{sat}$ and rhodium-plated titanium the counter electrode, connected to a potentiostat-galvanostat, AUTOLAB PGSTAT302N. Initially, the monitoring of the open circuit potential (OCP) of the samples was carried out for 60 min in the electrolyte, 0.1 mol/L NaCl, followed by EIS measurements with a disturbance amplitude of 10 mV (rms), in the frequency range from 100 kHz to 10 mHz with 10 points per logarithmic decade, soon after measurements of linear polarization resistance (R_{pl}) took place with a scan rate of 0.0167 mV/s in the range of $\pm$ 20 mV of the OCP. Finally, the potentiodynamic polarization curves were obtained with a scan rate of 0.167 mV/s and an overvoltage range of $\pm$ 250 mV vs OCP.

Figure 1. SBA-15, obtained after calcination.

2.8. Chemical characterization by fourier transform infrared spectroscopy (FTIR)

Films in the absence and presence of the best EXSBA concentration obtained by electrochemical tests (3%) were chemically evaluated by FTIR in a Bruker Alpha II equipment. The transmittance spectra were obtained in ATR mode in the wavenumber range from 4000 cm^{-1} to 650 cm^{-1} with a resolution of 4 cm^{-1}.

2.9. Morphological characterization by scanning electron microscopy (SEM/EDS)

Surfaces pretreated in the absence and presence of the best EXSBA concentration obtained by electrochemical tests (3%) were characterized by SEM (Tescan Vega3) and mapped with coupled energy dispersive X-ray spectroscopy (EDS), Oxford Instruments PentaFET Precision.

3. Results and Discussion

3.1. Characterization of SBA-15

3.1.1. X-ray diffraction analysis

Figure 2 shows the X-ray diffraction patterns of the SBA-15 sample after synthesis (SBA) and the SBA-15 sample after loading with the cocoa husk extract (EXSBA).

At low angles, the organization of the pores can be analyzed. The planes with Miller indices (100), (110), and (200) are the three characteristic peaks of the hexagonal mesostructure with 2D symmetry (p6mm) typical of SBA-15 found in the literature[26,32-34]. These peaks can be observed for the SBA-15 samples (Figure 2A) and are also maintained in the EXSBA-15 spectrum (Figure 2B). In addition, it is suggested that the decrease in the peak intensity (Figure 2B) occurred due to the presence of organic compounds from the cocoa husk extract in EXSBA, which causes disorder in the structure due to the loading. This behavior was observed by Liédana et al.[35] in the loading of SBA-15 with caffeine, and by Atiyah et al.[29], who associated the decrease in the

intensity of these peaks after loading with the presence of curcumin and organic groups in the microchannels.

The amorphous behavior of silica was identified by the presence of a band between 20° and 30° and the absence of other peaks. The presence of these bands is observed in the high-angle region in Figure 2A for SBA, and the same behavior is observed in Figure 2B for EXSBA, indicating that the characteristic of amorphous silica typical of SBA-15 was obtained and maintained after loading[36-38].

3.1.2. Morphological characterization

Figure 3 shows the SEM images of SBA (A) and EXSBA (B) at magnifications of 500 x and 10,000 x.

Figure 3A shows that the structure at lower magnification for the SBA has the appearance of fibers, while at higher magnification the presence of intertwined ropes with long channels is noted. EXSBA (Figure 3B) presents a similar morphological pattern to SBA, which indicates that there was no damage to the structure after loading with cocoa husk extract, corroborating the XRD analysis (Figure 2). The literature reports that the characteristic morphology of SBA-15 appears as sticks, intertwined ropes, or clusters of fibers of relatively uniform sizes[28,32], as seen in Figure 3. According to Meynen et al.[26], morphology can be changed during synthesis by adding salts or controlling nucleation through agitation, which can make channel rods shorter or straighter, which was not observed in Figure 3B, since the presented structure showed no change.

3.1.3. Chemical characterization

Figure 4 shows the normalized transmittance spectra obtained by FTIR for the EX (cocoa husk alcoholic extract), SBA, and EXSBA samples.

Figure 4 shows the presence of a broadband in the region of wavenumber 3286 cm^{-1} corresponding to the stretching vibration of the O-H bond in the residual water (SBA or EXSBA) or alcohol from the EX, the broadband in 3286 cm^{-1} and at 964 cm^{-1} corresponding to the stretching vibration of the O-H bond in the silanol group[39,40]. Si-H bonds can be found at 800 cm^{-1} relative to bending vibrations.
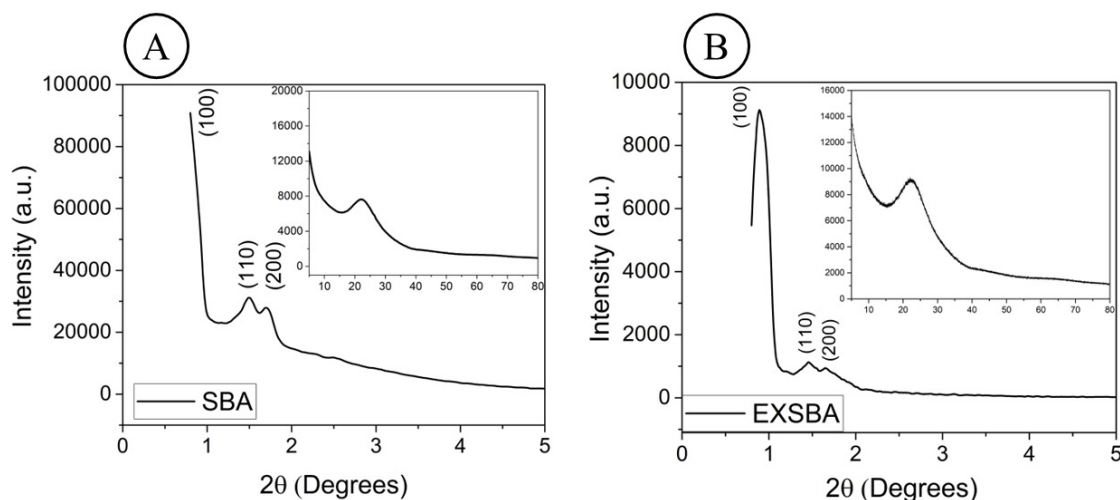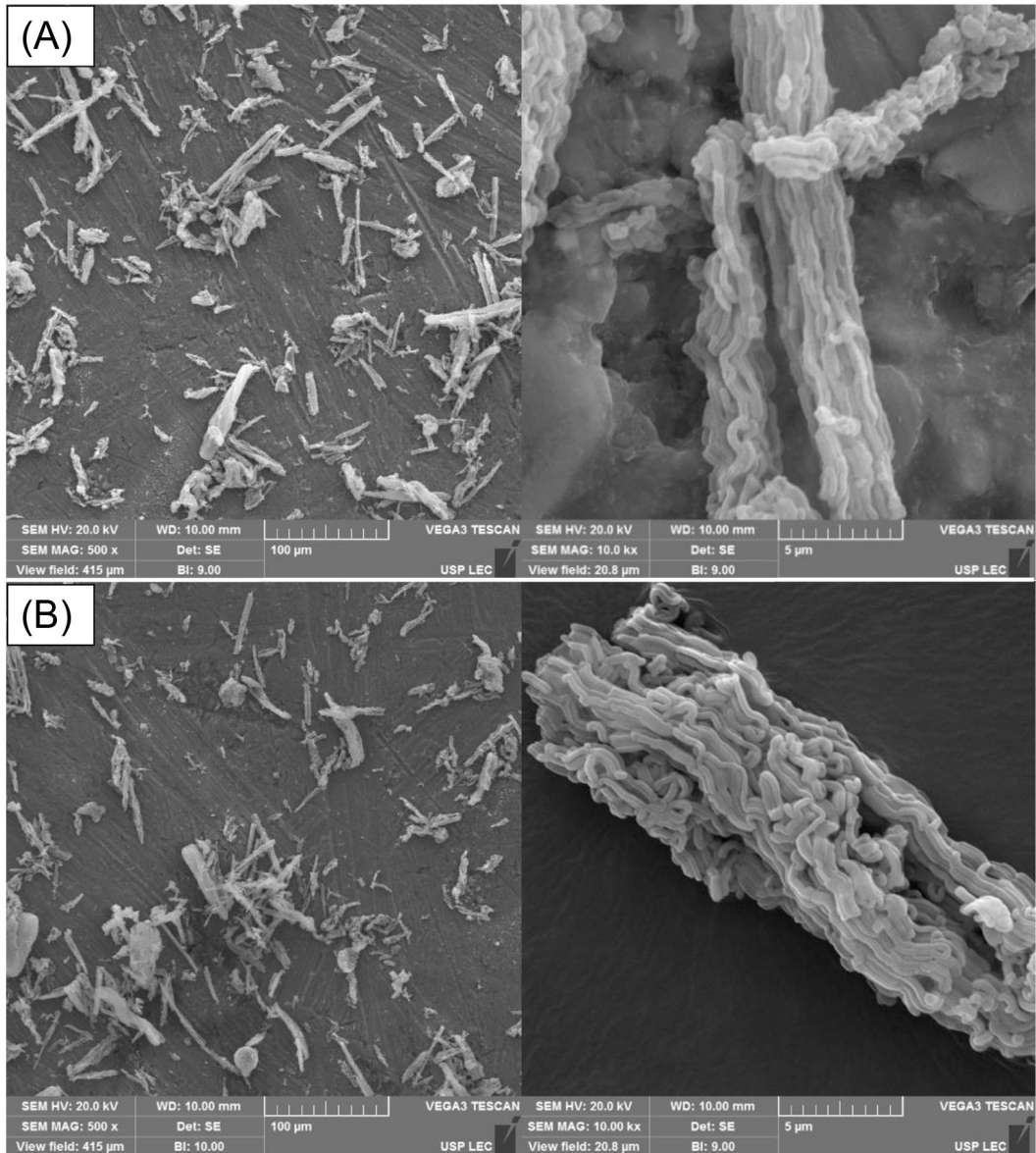

Figure 2. X-ray diffraction patterns of SBA (A) and EXSBA (B).

Figure 3. Images obtained by SEM of the SBA (A) and the EXSBA (B), the images follow magnification of 500 x and 10,000 x.

In addition, the spectra of SBA and EXSBA show the highest intensity at 1061 cm^{-1}, indicating stretching vibrations of the Si-O bonds of the siloxanes that can overlap in nearby bands[39,40]. The spectra of SBA-15 before (SBA) and after loading (EXSBA) showed the characteristic bond bands of the spectra found in the literature for SBA-15[29,33,41].

Atiyah et al.[29] observed the absence of new peaks in the spectra when comparing functionalized SBA-15 with functionalized SBA-15 loaded with curcumin and then related the increase in the intensity of the bands to the presence of functional groups of the curcumin, similarly Liédana et al.[35] observed when associating the spectra of SBA-15 with SBA-15 loaded with caffeine. In Figure 4, no new peaks were observed for EXSBA, but an increase in intensity was observed in the bands 3286 cm^{-1}, 1640 cm^{-1}, 1061 cm^{-1}, 964 cm^{-1}, and 800 cm^{-1}.
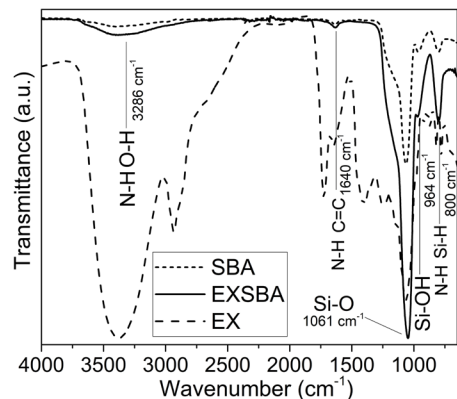
Figure 4. Normalized transmittance spectra of EX (cocoa husk alcoholic extract), SBA, and EXSBA samples.

The wavenumber region of 3286 cm⁻¹ is associated with symmetric and asymmetric stretching vibrations of the N-H bonds of primary and secondary amine groups, at 1640 cm⁻¹ with the angular bending of the N-H bonds of primary amines, the band at 800 cm⁻¹ refers to symmetric out-of-plane angular deformation (bending) for N-H bonds of primary and secondary amides. The stretching vibration of the C=C bonds of olefinic alkenes occurs in the region of 1640 cm⁻¹, at 964 cm⁻¹ and 800 cm⁻¹ the out-of-plane bending vibrations of the C-H bonds of these alkenes occur, and also at 800 cm⁻¹ vibrations out-of-plane bending of C-H bonds of aromatic hydrocarbons. Furthermore, in the band regions at 1245 cm⁻¹ and 1061 cm⁻¹ there are asymmetric stretching vibrations of the C-O-C ether bonds, and at 1061 cm⁻¹ symmetric stretching vibrations of the C-O-C ether bonds[11,40]. These bonds can contribute to the intensity of the bands in the EXSBA sample and are characteristics of molecules with inhibitory potential such as tannins, caffeine, theobromine, fatty acids, cellulose, hemicellulose, and lignin which are already widely reported in the literature to be present in the cocoa husk[11,42-44].

3.1.4. Thermogravimetric analysis

Figure 5 shows the curves obtained by thermogravimetric analysis for SBA and EXSBA samples.

The TG curve presented in Figure 5A indicates an initial thermal event related to the desorption of physisorbed water between the temperatures of 30 °C and 150 °C, in which a mass loss of 8.5% occurs in SBA. For EXSBA (Figure 5B), this same thermal event leads to a mass loss of 6.8%. Zambrano-Mite et al.[44] evaluated the thermal decomposition behavior of organic compounds from cocoa husk and associated this first stage of mass loss also with low molecular weight organic compounds. Therefore, the present work can also associate the mass loss in this first stage with the volatilization of these low molecular weight organic compounds that may be incorporated into EXSBA due to the loading with cocoa husk extract. The curve of SBA (Figure 5A) maintains the inorganic characteristic of thermal stability up to 800 °C, with a mass loss of 1.5% that can be attributed to the dehydroxylation of the mesoporous silica[45]. Therefore, there was a total mass loss of 10% for pure SBA-15.

EXSBA has another thermal event by DTG (Figure 5B), the second event occurs in the temperature range of 150 °C to 550 °C, with a mass loss of 7.4% which can be attributed to the degradation of high molecular weight organic components with possible inhibitory properties impregnated in the mesopores and micropores of EXSBA, such as: hemicellulose, cellulose, lignin, fatty acids and tannins[42,44]. Finally, an inorganic thermal behavior of mass loss is observed[44,45]. Thus, the total mass loss of EXSBA was about 14.2%, indicating that at least about 7.4% can be attributed to the presence of organic compounds within the pores of EXSBA.

3.2. Analysis and characterization of silane films

3.2.1. Electrochemical evaluation

Table 1 presents the sample abbreviations and OCP vs Ag/AgCl/KCl$_{sat}$ values after 60 min of potential stabilization.

Table 1. OCP obtained after 60 minutes of immersion in NaCl 0.1 mol/L.

Sample	Description	OCP (V).
ASTM1008	Bare carbon steel	-0.435
T	TEOS pretreated carbon steel	-0.386
T1SBA	TEOS pretreated carbon steel modified with 1% SBA-15 unloaded	-0.504
T1EXSBA	TEOS pretreated carbon steel modified with 1% EXSBA-15	-0.583
T2EXSBA	TEOS pretreated carbon steel modified with 2% EXSBA-15	-0.540
T3EXSBA	TEOS pretreated carbon steel modified with 3% EXSBA-15	-0.681
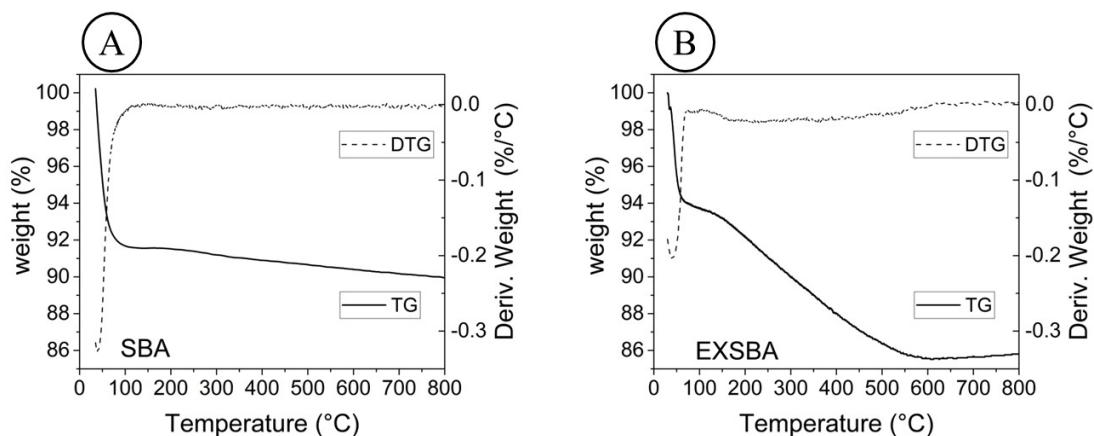
Figure 5. Thermogravimetric (TG) and Derivative Thermogravimetric (DTG) curves for SBA (A) and EXSBA samples (B).

The difference in the OCP value after 60 min from the pretreated samples to the bare steel indicates a change in the surface of these samples, shifted towards anodic or cathodic potentials compared to bare steel, suggesting the deposition of a film on the metallic surface[5,13].

Figure 6 shows the diagrams obtained by EIS after the stabilization of the open circuit potential.

The Nyquist diagram (Figure 6A) shows a single capacitive arc for the studied samples, with the smallest diameter of the semicircle for the T1SBA sample. This indicates a surface unprotected from the barrier effect, possibly due to the presence of pores of the SBA that facilitated the penetration of the electrolyte into the film and diffusion of the oxidizing agent on the metal surface. The samples modified with EXSBA showed an increase in the capacitive arc compared to the T sample, with a point marked at low frequency (31 mHz) associated with film/electrolyte interfacial reactions, which suggests an increase in corrosion resistance due to the presence and increasing the concentration of EXSBA in the TEOS silane film. The Bode diagram, impedance modulus (Figure 6B), shows the highest impedance modulus at low frequencies for the T3EXSBA sample, which indicates an improvement in the barrier effect promoted by the film in this condition. The Bode diagram, phase angle (Figure 6C), shows the highest phase angle values per low-frequency range for the T3EXSBA sample, which indicates an improvement in

the barrier effect promoted by this film. Still, in the T1SBA sample, a second time constant at high frequencies can be observed which may indicate oxide deposition on the surface due to the mesoporosity that facilitates the penetration of the electrolyte.

Table 2 presents the measurements of linear polarization resistance, R_{pl} for bare steel and pretreated samples, obtained after EIS measurement or 75 min of contact with the 0.1 mol/L NaCl solution.

The R_{pl} values observed in Table 2 increase as the concentration of EXSBA in the film increases, with the highest value presented for the T3EXSBA sample of 5.173 kΩ.cm² and the lowest value for the T1SBA sample, corroborating the results from EIS.

Table 2. R_{pl} of the bare steel sample and pretreated samples.

Sample	R_{pl} (kΩ.cm²)
ASTM1008	3.098
T	3.118
T1SBA	1.283
T1EXSBA	3.823
T2EXSBA	4.472
T3EXSBA	5.173
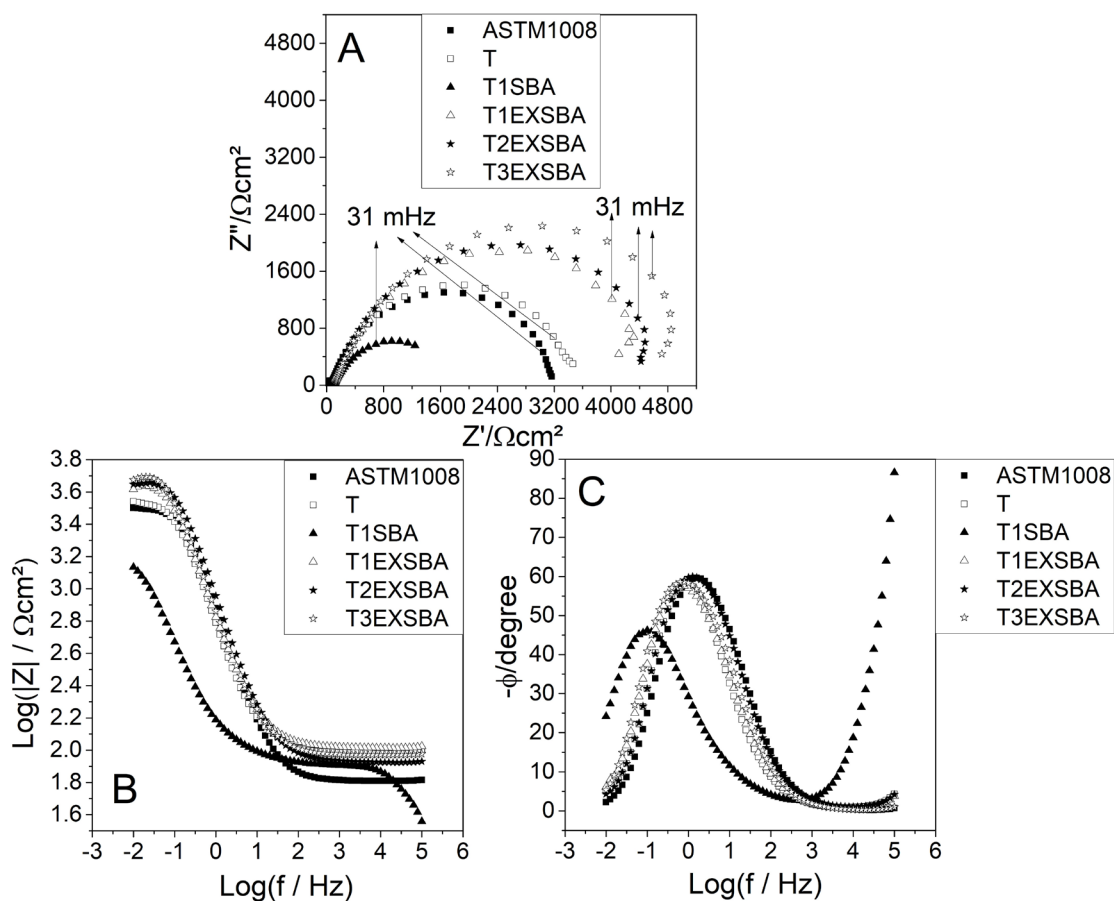
Figure 6. Nyquist (A), Bode impedance modulus (B) and Bode phase angle (C) diagrams for bare carbon steel and all pretreated samples.

Figure 7 presents the potentiodynamic polarization curves obtained after 80 min of contact with the electrolyte for the bare and pretreated carbon steel samples under the different studied conditions.

The polarization curves presented in Figure 7 indicated a decrease in corrosion current density for the samples pretreated with the TEOS film and modified with the loaded SBA-15, with the lowest anodic and cathodic corrosion current densities expressed for the T3EXSBA sample that may indicate the presence of a barrier effect promoted by the film[12,13]. The corrosion current density (i_{corr}) can be correlated with the R_{pl}, which i_{corr} is smaller for the T3EXSBA condition as R_{pl} increases. The corrosion potentials for samples pretreated with the film modified with EXSBA are shifted to more negative values compared to the ASTM1008 and T sample, indicating that the modified film delays the evolution of the corrosion process by electrolyte penetration, and the inhibitor present in EXSBA-15 acts preferentially in the cathodic reduction reactions[12,46].

3.2.2. Chemical characterization

Figure 8 shows the normalized transmittance spectra obtained by FTIR for the TEOS and TEOS films modified with 3% EXSBA, being the condition with the best electrochemical performance.

Initially, Figure 8 shows the broadband in the region of 3286 cm^{-1} referring to the stretching vibration of the O-H bond present in the film in the T sample and also to the chemical structure of EXSBA, or for the T3EXSBA sample the small increase in intensity in this region may be due to the presence of compounds from the cocoa husk extract such as theobromine or cellulose. The peak at 1061 cm^{-1} can be associated with stretching vibrations of the Si-O bonds of siloxanes present in the crosslinked film and in the structure of SBA-15, the higher intensity in the T3EXSBA sample which may suggest better film crosslinking with the interaction of EXSBA with the TEOS film. The peak at 964 cm^{-1} is related to silanols groups and is weaker for T3EXSBA due to more silanols groups present in the pure T sample. Finally, a characteristic peak at 800 cm^{-1} of the bending vibrations of the Si-H bonds present in the TEOS film and in EXSBA is observed[24,39,40].

3.2.3. Morphological characterization

Figure 9 shows images obtained by SEM for sample T (Figure 9A) and T3EXSBA (Figure 9B) using secondary (top images) and backscattered (bottom images) electron detectors. Figure 10 shows the maps obtained by EDS of the T sample surface and Figure 11 shows the maps of the T3EXSBA sample for the composition of silicon, oxygen, carbon, and iron.

Secondary electrons generated the micrograph shown in the upper part of Figure 9 and reveal a topography with roughness characteristics of bare carbon steel for the T sample (Figure 9A), as observed by Santos et al.[5], for bare carbon steel, in addition to the presence of the morphology of EXSBA precipitated on the surface of the T3EXSBA sample (Figure 9B). In the images generated by backscattered electrons, in the lower part of Figure 9, the lighter regions are related to elements of higher atomic

mass such as iron in the metallic alloy. In contrast, darker regions can be associated with the presence of lighter atoms such as silicon, carbon, and oxygen in the silane. Therefore, analyzing the composition in the images obtained by backscattered electrons, due to the presence of lighter regions in Figure 9A, compared to Figure 9B, the surface presents no homogeneity of the film based on TEOS silane (Figure 9), which can also be seen on the EDS map of that surface in Figure 10. The T3EXSBA sample in Figure 9B, when compared to the T sample in Figure 9A, for the backscattered electron image, presents a darker and more homogeneous contrast on the surface where EXSBA adhered, which indicates an improvement in the adsorption of the TEOS film on the surface, as well as an interaction between EXSBA and the silane, being verified with the EDS map in Figure 11 in which the T3EXSBA sample has less iron presence that improved surface coverage.
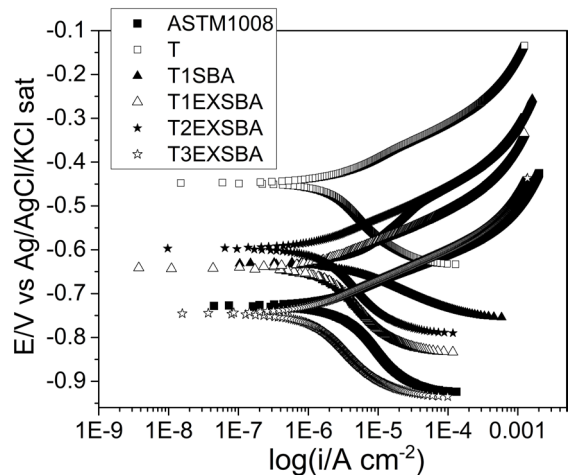

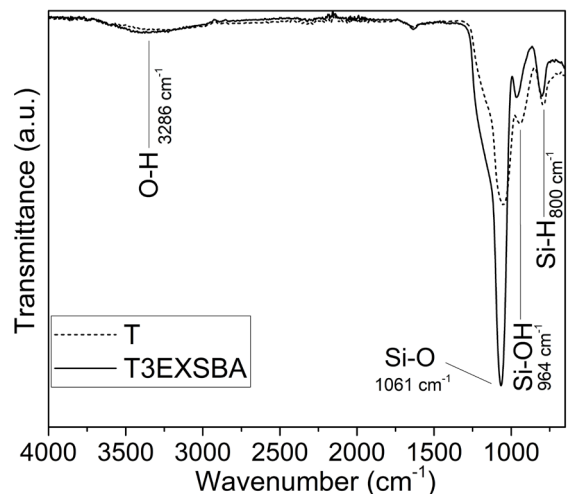**Figure 7.** Tafel potentiodynamic polarization curves for bare and pretreated carbon steel samples.

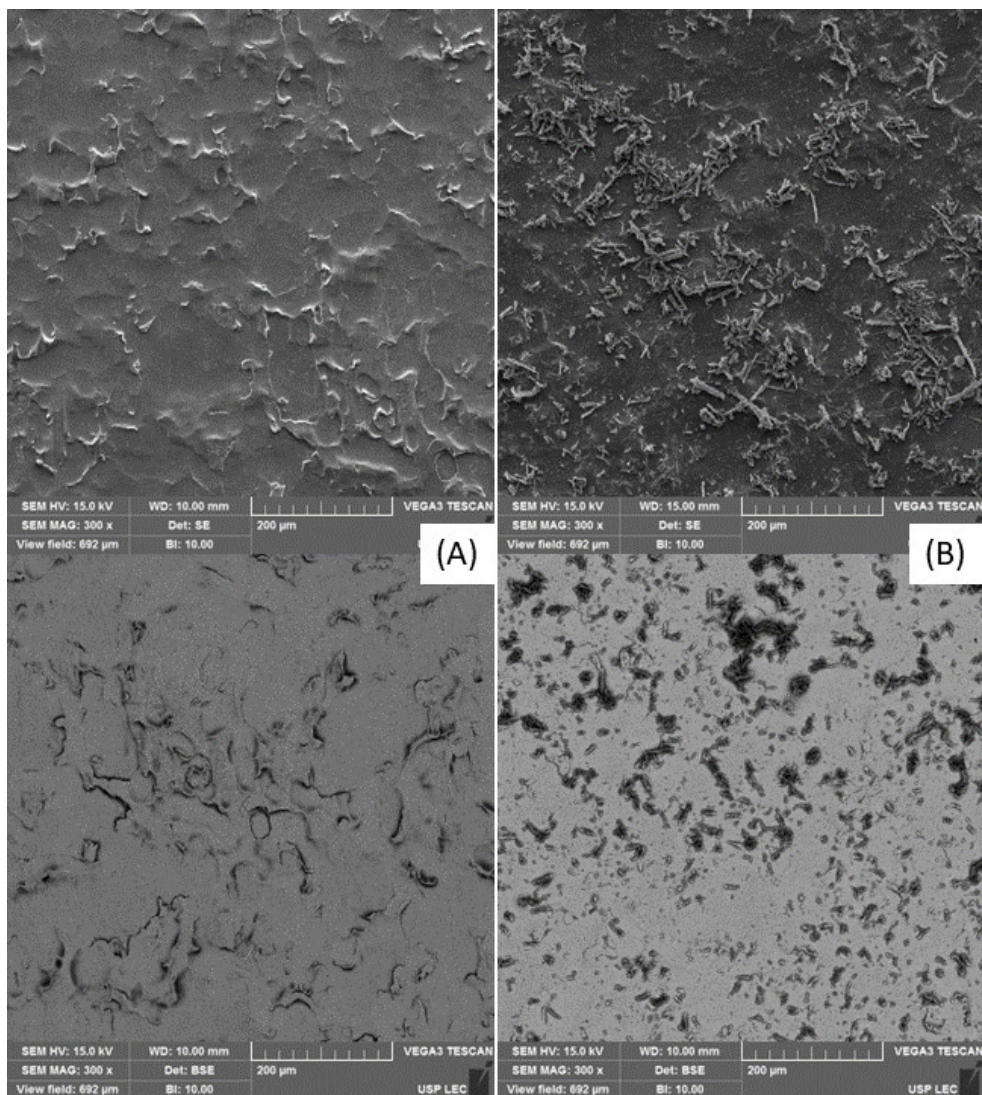**Figure 8.** Normalized transmittance spectra of T and T3EXSBA films.

Figure 9. SEM images of the T sample (A) and the T3EXSBA sample (B).
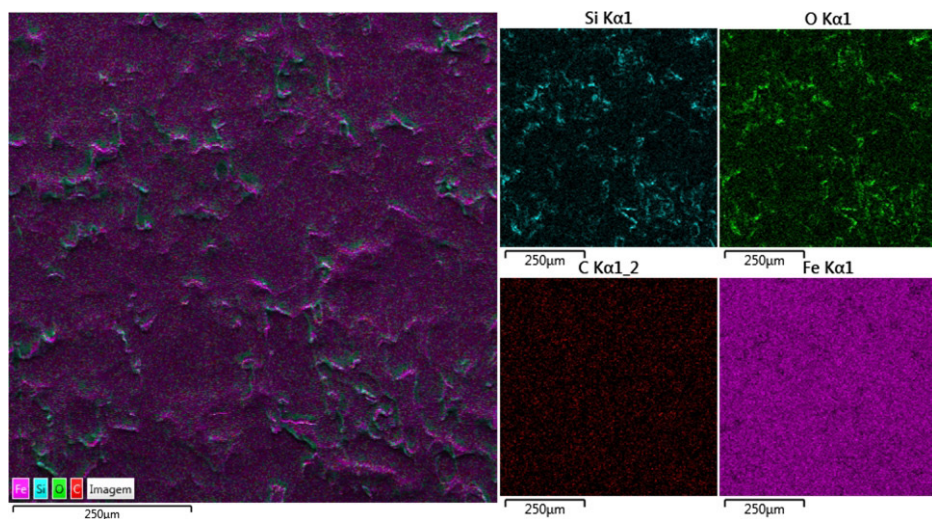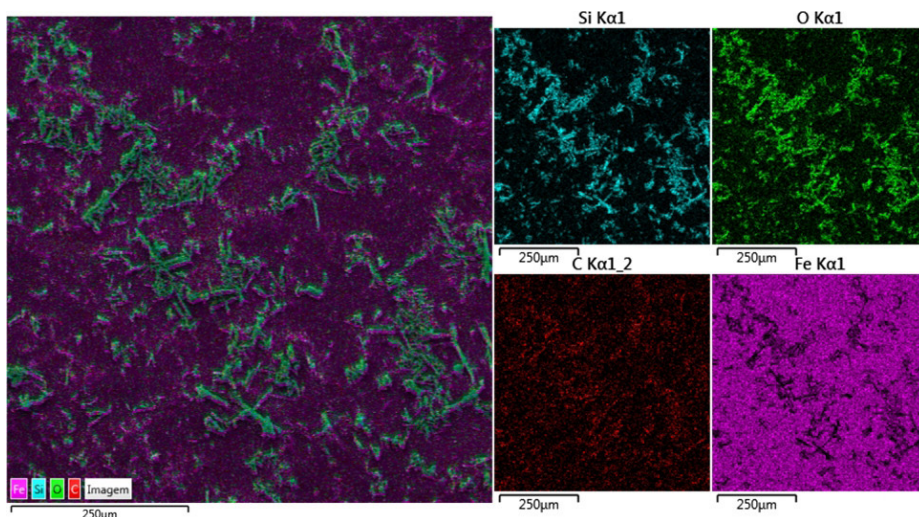

Figure 10. T sample EDS map.

Figure 11. T3EXSBA sample EDS map.

4. Conclusion

From the application of a residue as a sustainable inhibitor, cocoa husk, a pretreatment with improved electrochemical performance was developed by introducing 3% (wt%) of SBA-15 loaded with the alcoholic extract of the cocoa husk powder into a TEOS silane film for protection against corrosion of ASTM1008 steel in 0.1 mol/L NaCl solution. A notable limitation of this work is the precise quantification of the natural inhibitor loaded on SBA-15.

5. Acknowledgments

6. References

1. Singh A, Ansari KR, Haque J, Dohare P, Lgaz H, Salghi R, et al. Effect of electron donating functional groups on corrosion inhibition of mild steel in hydrochloric acid: experimental and quantum chemical study. J Taiwan Inst Chem Eng. 2018;82:233-51.

2. Prabakaran M, Kim SH, Hemapriya V, Chung IM. Tragia plukenetii extract as an eco-friendly inhibitor for mild steel corrosion in HCl 1 M acidic medium. Res Chem Intermed. 2016;42:3703-19.

3. Martin U, Bastidas DM. Stress corrosion cracking failure analysis of AISI 1018 carbon steel reinforcing bars in carbonated and chloride contaminated environment. Eng Fail Anal. 2023;147:107159. http://dx.doi.org/10.1016/j.engfailanal.2023.107159.

4. Yeganeh M, Asadi N, Omidi M, Mahdavian M. An investigation on the corrosion behavior of the epoxy coating embedded with mesoporous silica nanocontainer loaded by sulfamethazine inhibitor. Prog Org Coat. 2019;128:75-81.

5. Santos SLBS, da Silva BP, Tokumoto MS, de Freitas FG, Aoki IV, Capelossi VR. Pretreatment of carbon steel with silane film modified with a mixture of garlic and cocoa. J Sol-Gel Sci Technol. 2023;107:771-82. http://dx.doi.org/10.1007/s10971-023-06154-2.

6. Alcantara-Garcia A, Garcia-Casas A, Jimenez-Morales A. The effect of the organosilane content on the barrier features of sol-gel anticorrosive coatings applied on carbon steel. Prog Org Coat. 2019;139. http://dx.doi.org/10.1016/j.porgcoat.2019.105418.

7. Alibakhshi E, Ghasemi E, Mahdavian M, Ramezanzadeh B. Fabrication and characterization of layered double hydroxide/silane nanocomposite coatings for protection of mild steel. J Taiwan Inst Chem Eng. 2017;80:924-34.

8. Santos SLBS, de Freitas FG, Benvenuti T, Capelossi VR. TEOS/GPTMS Silane Sol-Gel Hybrid Film for Corrosion Protection of Carbon Steel. In: Baskar C, Ramakrishna S, La Rosa AD, editors. Encyclopedia of green materials. Singapore: Springer; 2022, p. 1-6.

9. Verma C, Ebenso EE, Quraishi MA. Corrosion inhibitors for ferrous and non-ferrous metals and alloys in ionic sodium chloride solutions: a review. J Mol Liq. 2017;248:927-42.

10. Periñán DEP, Vásquez MAV, Castellar PJM, Astudillo ICP. Evaluation of theobroma cacao pod husk extracts as corrosion inhibitor for carbon steel. CT&F Cienc Tecnol Futuro. 2016;6:147-56.

11. Barreto LS, Tokumoto MS, Guedes IC, de Melo HG, Amado F, Capelossi VR. Study and assessment of the efficiency of the cocoa bark extracted from the theobroma cacao as an inhibitor of the corrosion of carbon steel in substitution of benzotriazole. Mater Res. 2018;21:1-9.

12. Hamidon TS, Hussin MH. Susceptibility of hybrid sol-gel (TEOS-APTES) doped with caffeine as potent corrosion protective coatings for mild steel in 3. 5 wt. % NaCl. Prog Org Coat. 2020;140:105478.

13. Nikpour S, Naderi R, Mahdavian M. Fabrication of silane coating with improved protection performance using Mentha longifolia extract. J Taiwan Inst Chem Eng. 2018;88:261-76.

14. Montemor MF, Trabelsi W, Zheludevich M, Ferreira MGS. Modification of bis-silane solutions with rare-earth cations for improved corrosion protection of galvanized steel substrates. Prog Org Coat. 2006;57:67-77.

15. Peng T, Man R. Rare earth and silane as chromate replacers for corrosion protection on galvanized steel. J Rare Earths. 2009;27:159-63.

16. Suegama PH, de Melo HG, Benedetti AV, Aoki IV. Influence of cerium (IV) ions on the mechanism of organosilane polymerization and on the improvement of its barrier properties. Electrochim Acta. 2009;54:2655-62.

17. Mahdi AE, Ali NS, Majdi HS, Albayati TM, Abdulrahman MA, Jasim DJ, et al. Effective adsorption of 2-nitroaniline from wastewater applying mesoporous material MCM-48: equilibrium, isotherm, and mechanism investigation. Desalination Water Treat. 2023;300:120-9.

18. Albayati TM. Application of nanoporous material MCM-41 in a membrane adsorption reactor (MAR) as a hybrid process for removal of methyl orange. Desalination Water Treat. 2019;151:138-44.

19. Albayati TM, Sabri AA, Abed DB. Functionalized sba-15 by amine group for removal of ni(Ii) heavy metal ion in the batch adsorption system. Desalination Water Treat. 2020;174:301-10.

20. Albayati TM, Sabri AA, Abed DB. Adsorption of binary and multi heavy metals ions from aqueous solution by amine functionalized SBA-15 mesoporous adsorbent in a batch system. Desalination Water Treat. 2019;151:315-21.

21. Kalash KR, Albayati TM. Remediation of oil refinery wastewater implementing functionalized mesoporous materials mcm-41 in batch and continuous adsorption process. Desalination Water Treat. 2021;220:130-41.

22. Jafari-Tarzanagh Y, Seifzadeh D, Khodayari A, Samadianfard R. Active corrosion protection of AA2024 aluminum alloy by sol-gel coating containing inhibitor-loaded mesoporous SBA-15. Prog Org Coat. 2022;173:107166.

23. da Silva BP, Saji VS, Aoki IV. Rapid and eco-friendly one-step synthesis of dodecylamine-encapsulated mesoporous silica nanocontainers. Microporous Mesoporous Mater. 2022;341. http://dx.doi.org/10.1016/j.micromeso.2022.112109.

24. Tiringer U, Milošev I, Durán A, Castro Y. Hybrid sol–gel coatings based on GPTMS/TEOS containing colloidal SiO2 and cerium nitrate for increasing corrosion protection of aluminium alloy 7075-T6. J Sol-Gel Sci Technol. 2018;85:546-57.

25. Thai TT, Trinh AT, Olivier MG. Hybrid sol–gel coatings doped with cerium nanocontainers for active corrosion protection of AA2024. Prog Org Coat. 2020;138:105428.

26. Meynen V, Cool P, Vansant EF. Verified syntheses of mesoporous materials. Microporous Mesoporous Mater. 2009;125:170-223.

27. Amini M, Naderi R, Mahdavian M, Badiei A. Effect of piperazine functionalization of mesoporous silica Type SBA-15 on the loading efficiency of 2-Mercaptobenzothiazole corrosion inhibitor. Ind Eng Chem Res. 2020;59:3394-404.

28. Aliyeva N, Canak TC, Serhatlı İE. Synthesis and characterization of boron-acrylate/Santa Barbara Amorphous-15 polymer composite. J Appl Polym Sci. 2021;138:1-11.

29. Atiyah NA, Albayati TM, Atiya MA. Interaction behavior of curcumin encapsulated onto functionalized SBA-15 as an efficient carrier and release in drug delivery. J Mol Struct. 2022;1260:132879.

30. Barreto LS, Gonçalves GAC, Cotting F, Capelossi VR. Agro-industrial residues and plant biomass as green corrosion inhibitors. In: Baskar C, Ramakrishna S, La Rosa AD, editors. Encyclopedia of green materials. Singapore: Springer; 2022. p. 1-9.

31. Carvalho MCF, Silva IMFCR, Macedo PLA, Tokumoto MS, Cruz RS, Capelossi VR. Assessment of the hydroalcoholic extract and powder cocoa bean shell as corrosion inhibitors for carbon steel in sodium chloride solution. Revista Materia. 2021;26(2):e12978. http://dx.doi.org/10.1590/S1517-707620210002.1278.

32. Falcón JM, Otubo LM, Aoki IV. Highly ordered mesoporous silica loaded with dodecylamine for smart anticorrosion coatings. Surf Coat Tech. 2016;303:319-29.

33. Yuhua H, Xiaogang L, Minxin S, Yuanyuan Q, Xiancai L. Study on the adsorption of lanthanum ion imprinted on SBA-15/Y. J Indian Chem Soc. 2022;99:100425.

34. Zare-Dorabei R, Jalalat V, Tadjarodi A. Central composite design optimization of Ce(iii) ion removal from aqueous solution using modified SBA-15 mesoporous silica. New J Chem. 2016;40:5128-34.

35. Liédana N, Marín E, Téllez C, Coronas J. One-step encapsulation of caffeine in SBA-15 type and non-ordered silicas. Chem Eng J. 2013;223:714-21.

36. Amalorpavadoss A, Kumar S, Pavunkumar V, Chandramohan A, Dinakaran K, Harichandran G. Synthesis, Characterization and anti-corrosion property of GPTMS functionalized mesoporous silica (F-SBA-15) incorporated aliphatic chain containing polybenzoxazine nanocomposites. Compos Interfaces. 2022;29:833-52.

37. El-Lateef HMA, Khalaf MM. Novel dispersed Tl2O3-SiO2/polyaniline nanocomposites: in-situ polymerization, characterization and enforcement as a corrosion protective layer for carbon-steel in acidic chloride medium. Colloids Surf A Physicochem Eng Asp. 2019;573:95-111.

38. Zhang H, Xiao Z, Yang M, Zou J, Liu G, Zhang X. Highly dispersible cerium-oxide modified Ni/SBA-15 for steam reforming of bio-mass based JP10. Chin J Chem Eng. 2022;43:255-65.

39. Amini M, Naderi R, Mahdavian M, Badiei A. Release of lanthanum cations loaded into piperazine-modified SBA-15 to inhibit the mild steel corrosion. Microporous Mesoporous Mater. 2021;315:110908.

40. Silverstein RM, Webster FX, Kiemle DJ. Spectrometric identification of organic compounds. 7th ed. Hoboken: John Wiley & Sons; 2005.

41. Fan X, Wang X, Zhou D, Fan Y, Liu W, Hu W, et al. Screening of α-glucosidase inhibitors in tea by amino-functionalized mesoporous SBA-15 immobilized α-glucosidase microreactor. Microporous Mesoporous Mater. 2023;359. http://dx.doi.org/10.1016/j.micromeso.2023.112656.

42. Adjin-Tetteh M, Asiedu N, Dodoo-Arhin D, Karam A, Amaniampong PN. Thermochemical conversion and characterization of cocoa pod husks a potential agricultural waste from Ghana. Ind Crops Prod. 2018;119:304-12.

43. Campos-Vega R, Nieto-Figueroa KH, Oomah BD. Cocoa (Theobroma cacao L.) pod husk: renewable source of bioactive compounds. Trends Food Sci Technol. 2018;81:172-84.

44. Zambrano-Mite LF, Villasana Y, Bejarano ML, Luciani C, Niebieskikwiat D, Álvarez W, et al. Optimization of microfibrillated cellulose isolation from cocoa pod husk via mild oxalic acid hydrolysis: a response surface methodology approach. Heliyon. 2023;9. http://dx.doi.org/10.1016/j.heliyon.2023.e17258.

45. Sekkal KNEH, Ouargli-Saker R, Lachachi AK, Zekkari M, Beltrao-Nunes AP, Michelin L, et al. Effect of copper dispersion on SBA-15 and SBA-16 affinity towards carbon dioxide: an approach through thermal programmed desorption. J Nanopart Res. 2021;23:1-16.

46. Hernández-Barrios CA, Saavedra JA, Higuera SL, Coy AE, Viejo F. Effect of cerium on the physicochemical and anticorrosive features of TEOS-GPTMS sol-gel coatings deposited on the AZ31 magnesium alloy. Surf Interfaces. 2020;21. http://dx.doi.org/10.1016/j.surfin.2020.100671.